Journal of Geophysical Research: Oceans

RESEARCH ARTICLE
10.1029/2018JC014073

Temporal Variability in Surface Water pCO_2 in Adventfjorden (West Spitsbergen) With Emphasis on Physical and Biogeochemical Drivers

Y. Ericson[1,2], E. Falck[1,2], M. Chierici[1,3], A. Fransson[4], S. Kristiansen[5], S. M. Platt[6], O. Hermansen[6], and C. L. Myhre[6]

[1]Department of Arctic Geophysics, University Centre in Svalbard, Longyearbyen, Norway, [2]Geophysical Institute, University of Bergen, Bergen, Norway, [3]Institute of Marine Research, Fram Centre, Tromsø, Norway, [4]Norwegian Polar Institute, Fram Centre, Tromsø, Norway, [5]Department of Arctic and Marine Biology, UiT-The Arctic University of Norway, Tromsø, Norway, [6]NILU-Norwegian Institute for Air Research, Kjeller, Norway

Key Points:
- Large undersaturation of surface water pCO_2 with respect to atmospheric pCO_2 was observed in an Arctic fjord following two annual cycles
- Biological activity and temperature are key drivers for the observed monthly variability in surface water pCO_2
- The uptake of CO_2 is enhanced when Arctic origin waters are present in the fjord as compared to Atlantic origin waters

Correspondence to:
Y. Ericson,
ylva.ericson@unis.no

Citation:
Ericson, Y., Falck, E., Chierici, M., Fransson, A., Kristiansen, S., Platt, S. M., et al. (2018). Temporal variability in surface water pCO_2 in Adventfjorden (West Spitsbergen) with emphasis on physical and biogeochemical drivers. *Journal of Geophysical Research: Oceans*, *123*, 4888–4905. https://doi.org/10.1029/2018JC014073

Received 11 APR 2018
Accepted 14 JUN 2018
Accepted article online 26 JUN 2018
Published online 17 JUL 2018

Abstract Seasonal and interannual variability in surface water partial pressure of CO_2 (pCO_2) and air-sea CO_2 fluxes from a West Spitsbergen fjord (IsA Station, Adventfjorden) are presented, and the associated driving forces are evaluated. Marine CO_2 system data together with temperature, salinity, and nutrients, were collected at the IsA Station between March 2015 and June 2017. The surface waters were undersaturated in pCO_2 with respect to atmospheric pCO_2 all year round. The effects of biological activity (primary production/respiration) followed by thermal forcing on pCO_2 were the most important drivers on a seasonal scale. The ocean was a sink for atmospheric CO_2 with annual air-sea CO_2 fluxes of -36 ± 2 and -31 ± 2 g C·m^{-2}·year^{-1} for 2015–2016 and 2016–2017, respectively, as estimated from the month of April. Waters of an Arctic origin dominated in 2015 and were replaced in 2016 by waters of a transformed Atlantic source. The CO_2 uptake rates over the period of Arctic origin waters were significantly higher (2 mmol C·m^{-2}·day^{-1}) than the rates of the Atlantic origin waters of the following year.

1. Introduction

The West Spitsbergen fjords provide a unique and dynamic coastal environment, influenced by seasonal contributions of snow, glacial, and sea ice meltwaters (e.g., Cottier et al., 2005; Nilsen et al., 2008; Svendsen et al., 2002). These fjords are affected by the Atlantic Water (AW, $S > 34.9$) of the West Spitsbergen Current that flows north along the continental slope (Figure 1), as well as of the cold and fresh Arctic Water (ArW, $S < 34.7$) that flows northward on the shelf with the Coastal Current (e.g., Cottier et al., 2005; Nilsen et al., 2008). The former is typically mixed with the latter on the shelf and modified to Transformed Atlantic Water (TAW, $34.7 < S < 34.9$). The distribution and presence of these water masses inside the fjords vary with time (e.g., Cottier et al., 2005; Nilsen et al., 2008, 2016).

A few observations of the CO_2 system from West Spitsbergen fjords exist that show that the surface waters were undersaturated in the partial pressure of CO_2 (pCO_2) with respect to the atmospheric pCO_2 during the observed periods (Adventfjorden, Andersson et al., 2017; Kongsfjorden, Fransson et al., 2016; Tempelfjorden, Fransson et al., 2015), like most surface waters in the Arctic Ocean (e.g., Bates & Mathis, 2009; Jutterström & Anderson, 2010; Yasunaka et al., 2016). These areas have thereby the potential to act as net CO_2 sinks. A feature partly related to the temperature- and salinity-dependent solubility of CO_2, which reflects the cold and rather fresh surface layer of the Arctic. Still, Arctic coastal regions show great variability in surface water pCO_2 as well as in air-sea CO_2 fluxes, both in space and time (e.g., Else et al., 2013; Evans et al., 2015; Fransson et al., 2017; Pipko et al., 2011; Semiletov et al., 2007). This is intricately linked to local conditions of primary production/respiration, sea ice processes, terrestrial runoff, and vertical mixing, as observed in different regions of the Arctic Ocean (e.g., Chierici et al., 2011; Else et al., 2012; Fransson et al., 2013, 2017; Pipko et al., 2011; Sejr et al., 2011).

In waters north of Svalbard, the effect of sea ice processes on surface water pCO_2, mainly through the dissolution of calcium carbonate ($CaCO_3$) in the surface waters, dominates changes (i.e., undersaturation) in surface water pCO_2 on a 6 months' time scale (January to June, Fransson et al., 2017). Further south, in Isfjorden, the largest fjord along the West Spitsbergen coast, the amount of sea ice has decreased substantially over the last decade, both in terms of maximum sea ice cover and days of fast ice (Isaksen et al., 2016;

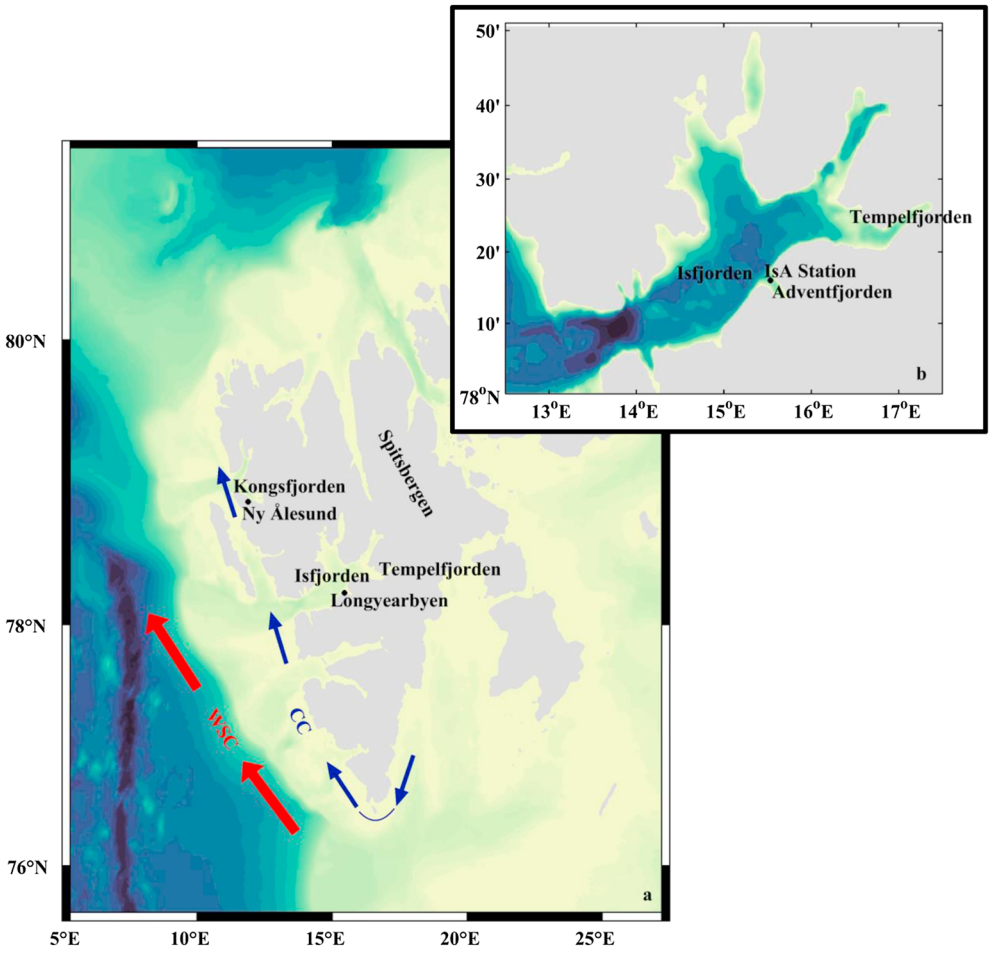

Figure 1. (a) Map of Spitsbergen showing Isfjorden, the locations of Ny Ålesund and Longyearbyen (black dots), and the surrounding shelf with the Coastal Current (CC) shown with blue arrows and the West Spitsbergen Current (WSC) depicted with red arrows, and, (b) map of Isfjorden showing the location of the IsA Station (N78°16.0, E15°32.0, with a depth of 94 m, black dot) in Adventfjorden.

Muckenhuber et al., 2016). This fjord is surrounded by glaciers and nearly 3000×10^6 m^3 of glacial meltwater feeds the system every year (Nilsen et al., 2008, and references therein). Studies from other glacier-influenced fjords in Svalbard (Fransson et al., 2015, 2016) and on the Greenland coast (Meire et al., 2015; Rysgaard et al., 2012) show that glacial meltwater may promote an uptake of CO_2 from the atmosphere.

The annual magnitude and the interannual variability of the CO_2 sink in the Isfjorden system are so far not well known. In the present study marine CO_2 system data from March 2015 to June 2017 from Adventfjorden (IsA Station, N78°16.0, E15°32.0, Figure 1), a small branch of the Isfjorden system, are presented and investigated. More specifically, the seasonal to interannual variability in surface water pCO_2 and the corresponding air-sea CO_2 fluxes are studied and the effects of key physical and biological drivers on the surface water pCO_2 are evaluated. In addition, the impact on the air-sea CO_2 fluxes between surface water of Arctic and Atlantic origins are compared.

2. Materials and Methods

2.1. Data Collection

Hydrographic work was carried out at the IsA Station between March 2015 and June 2017, in total 38 times during all seasons (see Table A1). Freshwater runoff was also collected from the Advent Valley riverbed in June 2015 (for total alkalinity [TA] and pH measurements). Temperature (T) and salinity (S) were measured using different types of conductivity-temperature-depth (CTD) devices (SAIV A/S SD204, Sea-Bird

SBE9/SBE37/SBE19+). From February 2016 and onward, the sampling was performed with a SBE19+ with a few exceptions. The SBE19+ was calibrated each year and cross-checked with the SD204 and SBE37. The SBE19+ has a better resolution and accuracy than the SD204 (see Table A2), and the two instruments were deployed together on four occasions. This resulted in corrections of −0.10, −0.13, and −0.14 of the salinity data obtained from the SD204 in spring 2016 (28 April), autumn 2016 (20 September), and spring 2017 (24 February, 21 March, and 3 April), respectively. The SD204 failed to log temperature on one occasion (22 April 2015). To be able to use the corresponding water samples that were collected on that occasion, CTD data collected 5 days earlier (17 April 2015) at the station were used instead, assuming little variability during the period.

Discrete samples of pH, TA, and nutrients (nitrate, phosphate) were collected typically using handheld Niskin bottles (1.7, 5 or 10 L). The surface sample was in general collected from 2 m. The pH/TA samples were transferred into rinsed 250-ml borosilicate bottles that were filled from the bottom. The water was allowed to overflow to flush out the water that had been in contact with air. Generally, these samples, with few exceptions, were analyzed the day after at the University Centre of Svalbard (UNIS), Longyearbyen, Norway. The nutrient samples were collected in 125-ml Nalgene® bottles and stored frozen.

pH was determined spectrophotometrically on the total hydrogen scale (pH_T) using the indicator *m*-cresol purple (*m*Cp, Clayton & Byrne, 1993). The perturbation of the sample pH as a result of the addition of the indicator was corrected for as suggested by Chierici et al. (1999). The precision, as estimated from the average of all absolute valued differences between duplicate sample runs, was ±0.001. The UNIS laboratory participated in a CO_2 interlaboratory comparison in May 2017, and both batches of unpurified *m*Cp used in this study were tested. In average the measured pH was 0.005 ± 0.001 higher than the certified value for ambient pCO_2 conditions.

TA was analyzed using a nonpurged open cell potentiometric method (Metrohm ©Titrando system, Switzerland). A nonlinear least squares optimization was used in the TA determination (Department of Energy, 1994). This method assumes no air-sample gas exchange. The impact of CO_2 loss on the TA calculation is minimal for titrations of ~3 min. For longer titrations, for example, 10 min, the calculated TA for a closed system is ~0.2% higher than the calculated TA for a system that includes gas exchange in the nonlinear least squares optimization. The method has a precision of around ±2 μmol/kg. For eight of the samples over the entire period the nonlinear least squares method failed due to noisy electrode response and an optimized endpoint determination was used (Metrohm ©tiamo™: titration software, Switzerland) with a precision of roughly ±4 μmol/kg. The average difference between the two methods was 2.0 ± 3.6 μmol/kg. The accuracy of the TA measurements was set by the use of Certified Reference Materials purchased from A. Dickson, Scripps Institution of Oceanography (United States). This one-point calibration largely removes the uncertainty in the calculated TA due to gaseous exchange. In the CO_2 interlaboratory comparison in 2017 the measured TA, using the nonlinear least square method and the endpoint determination, differed from the certified values with −0.1 ± 0.9 and 0.7 ± 0.8 μmol/kg, respectively.

The nutrient samples that were collected between April 2015 and May 2016, except for 2 May 2015, were measured at the Institute of Marine Research, Bergen, Norway. The detection limits for nitrate (NO_3^-) and phosphate (PO_4^{3-}) were 0.4 and 0.06 μmol/L, respectively. The samples from 2 May 2015 were analyzed at UiT The Arctic University of Norway. The detection limits for NO_3^- and PO_4^{3-} were 0.04 and 0.01 μmol/L, respectively. The remaining samples were analyzed at the UNIS, Longyearbyen, Norway. Here the detection limit was determined from blank measurements using a *t* test to 0.05 and 0.005 μmol/L for NO_3^- and PO_4^{3-}, respectively (n = 10, significance level: 0.01). Precision as estimated from duplicate sample runs was ±0.03 and ± 0.006 μmol/L for NO_3^- and PO_4^{3-}, respectively (n = 29). The nutrient data were converted to micromoles per kilogram using the sample density at 1 atm, in situ salinity, and a laboratory temperature measured at UNIS of 21°C, which was assumed to be comparable between laboratories.

2.2. Calculations of Surface Water pCO_2 and Air-Sea CO_2 Fluxes

The surface water pCO_2 and total dissolved inorganic carbon (DIC) were calculated from the combination of TA and pH together with the sea surface temperature (SST), sea surface salinity (SSS), and pressure data using CO2SYS MATLAB-version 1.1 (van Heuven et al., 2011). The DIC of the freshwater samples from the Advent Valley riverbed was also calculated using CO2SYS with K_1 and K_2 of Millero (1979). In terms of the seawater

samples, Chen et al. (2015) found that for Arctic surface waters the stoichiometric dissociation constants of carbonic acid (K_1 and K_2) of Mehrbach et al. (1973) as refit by Dickson and Millero (1987) and of Lueker et al. (2000) had the best agreement between calculated and measured pCO_2. This finding was also supported by the study of Woosley et al. (2017), although as pointed out by the authors, a better internal consistency does not necessarily guarantee a better accuracy. The K_1 and K_2 of Mehrbach et al. (1973) as refit by Dickson and Millero (1987), together with the dissociation constant of bisulphate (K_{SO4}) of Dickson (1990) and total borate according to Uppström (1974), were used in all further calculations of the inorganic carbon system using the CO2SYS script.

The uncertainties of the calculated pCO_2 and DIC at output condition with variations in input parameters (TA, pH, S, T, K_1, and K_2) were estimated in terms of $\left(\frac{\partial y}{\partial x_i}\right)$ referred to as the partial in the original CO2SYS software (Lewis & Wallace, 1998). Here the calculated property y represents either pCO_2 or DIC. The input parameters were treated as independent with the uncertainty calculated as follows:

$$(\delta y)^2 = \sum_i \left(\frac{\partial y}{\partial x_i}\delta x_i\right)^2 \tag{1}$$

where δx_i refers to the uncertainty/standard deviation of the measured property and δy refers to the uncertainty in the calculated variable. The uncertainties in the input parameters are presented in Table A2.

The bulk formula for air-sea CO_2 fluxes (F_{asf}) is commonly written as the product between the gas coefficient (kK_0) and the partial pressure difference between air (pCO_{2a}) and water (pCO_{2w}):

$$F_{asf} = kK_0(pCO_{2w} - pCO_{2a}) \tag{2}$$

where k is the gas transfer velocity (cm/hr) and K_0 is the solubility coefficient of CO_2 (mol·m^{-3}·atm^{-1}). K_0 was determined from in situ salinity and temperature according to Weiss (1974) who also suggested an uncertainty in the estimated K_0 in the order of 0.2%. The gas transfer velocity is a key uncertainty in bulk flux calculations. Unfortunately, there are no robust wind speed parameterizations of k that applies to the Arctic environment where wintertime convection is important (Andersson et al., 2017). For this work the formula of Wanninkhof (2014), which has an estimated uncertainty of 20% on a basin scale, was used:

$$k = 0.251 < U_{10}^2 > \left(\frac{Sc}{660}\right)^{-0.5} \tag{3}$$

where U_{10} is the wind speed at 10 m and Sc is the Schmidt number. The coefficient of 0.251 was estimated for the Cross-Calibrated Multi-Platform wind speed product, which does not cover the Arctic region. Still, the wind speed relationship of Wanninkhof (2014) agrees well with, among several others, the gas exchange study of Nightingale et al. (2000) from the North Sea, and the hybrid model of Wanninkhof et al. (2009) that includes nonwind effects on the gas transfer velocity such as chemical enhancement and buoyancy fluxes. Hourly measured wind speed data at 10 m from Svalbard Airport (Longyearbyen) were obtained from the Norwegian Meteorological Institute (eklima.met.no/). Monthly averages of the squared wind speed were calculated and used in equation (3). The seawater Schmidt number polynomial of Wanninkhof (2014) was used in the calculations.

Atmospheric pCO_2 data for use in equation (2) were obtained from the Zeppelin Mountain at 474 m in Ny Ålesund (Zeppelin Observatory, Spitsbergen, NILU-Norwegian Institute for Air Research, http://ebas.nilu.no/). The data are given as hourly averaged xCO_2 in dry air and hence must be converted to pCO_2 in wet air. To do this the following equation has been used:

$$pCO_2 = \left(P - p_{H_2O}\right)xCO_2 \tag{4}$$

where P is air pressure at sea level taken from Svalbard Airport and p_{H2O} is the vapor pressure calculated according to the World Meteorological Organization (2014, WMO-No. 8) using P, temperature, and relative humidity from Longyearbyen airport (data from the Norwegian Meteorological Institute, eklima.met.no/). Low-quality xCO_2 data (e.g., flagged with 682, standard deviation>1 μmol mol^{-1}, or outliers) were removed.

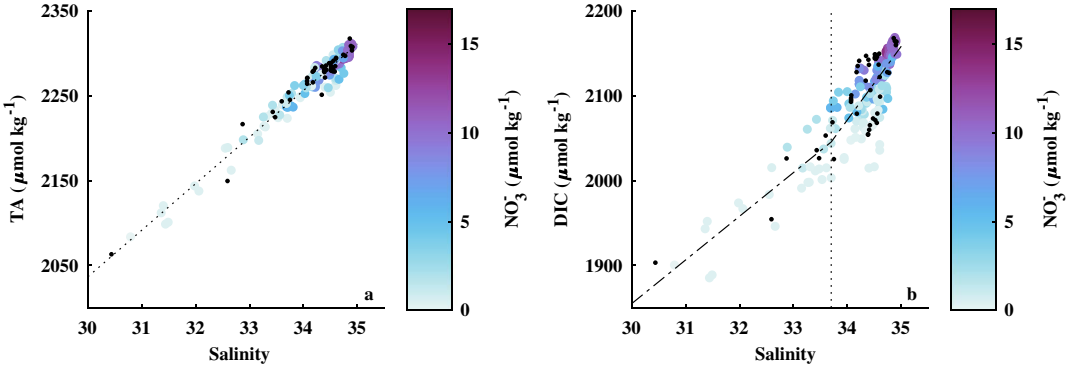

Figure 2. Plot of (a) TA versus salinity (linear equation: $y = 55.0 \cdot S + 387$, $R^2 = 0.96$) and (b) DIC versus salinity (break points: $DIC_{S=30} = 1{,}855.0$, $DIC_{S=33.7} = 2{,}045.7$, and $DIC_{S=35} = 2{,}158.8$, $R^2 = 0.78$). Coloring shows the NO_3^- concentration; black dots indicate no NO_3^- data. TA = total alkalinity; DIC = dissolved inorganic carbon.

The air-sea pCO_2 gradient was then calculated from the difference between the observed surface water pCO_2 and the atmospheric pCO_2 at the Zeppelin Station. At two occasions the atmospheric pCO_2 was linearly interpolated since there were some gaps in the data set. The uncertainty in these interpolated values should be reflected in the standard deviation of the atmospheric pCO_2 over a longer period, for example, a month, which typically varies around 4 μatm. This gives an uncertainty in the interpolated pCO_2 of ±1%.

The uncertainty in the estimated fluxes ranged between 20% and 33% as estimated from uncertainties in k, K_0, and the air-sea pCO_2 gradient of 20%, 0.2%, and 4–26%, respectively. The fluxes were integrated over the annual cycle using trapezoidal integration. The uncertainty in the annual flux was obtained by taking care of the error propagation at each area calculation and summation step of the trapezoidal integration.

2.3. Drivers of pCO_2 Variability

Variability in surface water pCO_2 can be explained by several processes of which thermal forcing, changes in salinity, mixing/advection, air-sea CO_2 fluxes, and biological forcing will be considered here. Since there was no sea ice in Adventfjorden apart from a brief period in mid-March 2015, changes in pCO_2 due to $CaCO_3$ dissolution/formation are omitted. Riverine input of TA and DIC are included in the assessment of mixing and advection, whereas riverine nutrients and organic matter will mainly be covered in the discussion section. The monthly effects of the individual processes on surface water pCO_2 were estimated as done previously by a number of authors (e.g., Chierici et al., 2006; Fransson et al., 2017; Lüger et al., 2004).

The change in pCO_2 as a result of a change in temperature is commonly estimated according to Takahashi et al. (1993):

$$\partial \ln pCO_2 / \partial T = 0.0423/^{\circ}\mathrm{C} \tag{5}$$

for salinities and temperatures of 34–36 and 2–28°C, respectively. To take into account the cold climate and seasonal discharges of freshwater at the study site, the temperature coefficient above (0.0423/°C) may not be valid. A model was therefore set up to estimate a value for colder (−1.8 and 10°C) and less saline waters ($30 < S < 35$) using CO2SYS with a resolution of 0.1 in salinity. For each step in salinity, TA and DIC were used to estimate pCO_2 for the temperature range −1.8 and 10°C. To see which TA and DIC values to use for the different salinity steps, all TA and DIC values are plotted against salinity in Figure 2. Typical TA and DIC values for the salinity range and resolution in question were obtained from linear regression. For the DIC data the regression was segmented with a break point at $S = 33.7$. The variability in DIC for $S > 33.7$ is affected by primary production to a larger degree then for $S < 33.7$ as indicated by the sharp decline in NO_3^- in the salinity range of 33.7 to 35 (Figure 2). A segmented regression for the DIC values therefor captures the natural variability better.

The relationship between the natural logarithm of pCO_2 for each salinity level and temperature was evaluated with a linear least square fit. The obtained temperature coefficients (β), that is, $\partial \ln pCO_2 / \partial T$, were

Table 1
Mean Temperature Coefficients (β) for Specific Salinity Intervals

Salinity	β ($^{\circ}C^{-1}$)
30–32	0.0459
32–33	0.0458
33–34	0.0457
34–34.5	0.0456
34.5–35	0.0454

binned to salinity intervals according to Table 1. The change in pCO_2 between two sampling occasions as a result of temperature changes ($\Delta pCO_{2,T}$) was then estimated for each salinity bin:

$$\Delta pCO_{2,T} = pCO_{2,pm} e^{\beta \Delta T} - pCO_{2,pm} \quad (6)$$

where β is taken from Table 1 according to the salinity, ΔT is the observed change in temperature between two sampling occasions, and pm denotes the previous measurement.

Changes in salinity also affect the solubility of CO_2, and this effect on pCO_2 was estimated according to equation (7) (Sarmiento & Gruber, 2006):

$$\Delta pCO_{2,S} = \Delta S \frac{pCO_{2,pm}}{S_{pm}} (\partial \ln pCO_2 / \partial \ln S)_{pm} \quad (7)$$

where S is salinity and ΔS is the observed change in salinity. Again, pm denotes the previous measurement.

When sea ice is absent, salinity varies mainly due to evaporation, precipitation, mixing between different water masses including freshwater runoff, and advection. These processes will also result in changes in TA and DIC, which consequently will affect the surface water pCO_2. This change in pCO_2 ($\Delta pCO_{2,mix,adv}$) was estimated from TA-S and DIC-S relationships:

$$TA = 57.5S + 294 \quad (8a)$$

$$DIC = 52.0S + 339 \quad (8b)$$

Changes in salinity (ΔS) between sampling occasions were used to calculate the corresponding changes in TA (ΔTA_s) and DIC (ΔDIC_s). ΔTA_s and ΔDIC_s were added to the TA and DIC of the previous occasion and the perturbed pCO_2 was calculated using CO2SYS for the salinity and temperature conditions of the previous sampling. The change in pCO_2 was determined from the difference between the perturbed pCO_2 and the pCO_2 of the previous sampling occasion. Equations (8a) and (8b) were derived for mixing between TAW (prebloom mean values from 2016: S = 34.8, TA = 2,295 μmol/kg, DIC = 2,150 μmol/kg) and land runoff (TA = 294 ± 3 μmol/kg, DIC = 339 ± 7 μmol/kg). The corresponding equations for mixing between ArW (i.e., prebloom values from 2015: S = 34.5, TA = 2276 μmol/kg, DIC = 2,140 μmol/kg) and land runoff differ by less than 1%, and no distinction is therefor made to discriminate between ArW and TAW. Furthermore, the $\Delta TA/\Delta S$ and $\Delta DIC/\Delta S$ ratios of equations (8a) and (8b) are 4% and 1% higher than the ratios of the linear relationship in Figure 2a and the segmented regression ($S < 33.7$) in Figure 2b, respectively. In comparison, the $\Delta TA/\Delta S$ and $\Delta DIC/\Delta S$ ratios of equations (8a) and (8b) are 15% and 19% lower, respectively, than the corresponding ratios for a purely precipitation/evaporation driven TA and DIC variability. This confirms that the effect of land runoff on the TA and DIC variability dominates over the effects of evaporation and precipitation.

The change in pCO_2 between observations due to air-sea exchange was estimated from the expression below:

$$\Delta pCO_{2,asf} = \int_{t_{pm}}^{t_m} F_{asf} dt \frac{(\partial \ln pCO_2 / \partial \ln DIC)_{pm}}{h_{BD}} \frac{pCO_{2,pm}}{DIC_{pm}} \quad (9)$$

using trapezoidal integration of the flux (F_{asf}, equation (2)) between sampling occasions, that is, between the previous measurement at time, t_{pm}, and the current measurement at time, t_m. Equation (9) is based on the assumption that the absorbed CO_2 is distributed over the equivalent to the mixed layer depth, h_{BD}, at time t_m. This property was developed by Randelhoff et al. (2017) for the marginal ice zone where the impact of sea ice melt results in a similar shift from a nonstratified to a stratified water column as observed in Svalbard fjords. h_{BD} can be regarded as an upper bound of the depth to which wind driven turbulent mixing reaches (Randelhoff et al., 2017). The authors defined the equivalent to the mixed layer depth using the potential density anomaly of seawater ($\sigma_\theta = \rho$ – 1,000 kg/m^3), according to the equation:

$$h_{BD} = BD / \Delta \sigma_\theta \quad (10)$$

where BD is the buoyancy deficit and $\Delta\sigma_\theta$ is the density difference between the surface (mean σ_θ over 3 to 5 m) and a deeper reference layer ($\sigma_{\theta d}$). The BD was calculated as follows:

$$\mathrm{BD} = \int_{\mathrm{Surface}}^{60\ \mathrm{m}} \mathrm{d}z[\sigma_{\theta \mathrm{d}} - \sigma_\theta(z)] \tag{11}$$

Based on visual inspection of all density profiles the background deep water density ($\sigma_{\theta d}$) was defined as the mean over the depth range of 55–65 m. If the surface density deviation $\Delta\sigma_\theta$ was larger than 0.03 kg/m^3 the profiles were considered to be influenced by freshwater. This limit was set to discern real differences in density from noise in the low resolution measurements of the SD204.

Biological activity, in terms of the balance between primary production and respiration in the surface waters, is reflected by changes in DIC according to the equation below:

$$\Delta p\mathrm{CO}_{2,\mathrm{bio}} = (\Delta\mathrm{DIC} - \Delta\mathrm{DIC}_{\mathrm{asf}} - \Delta\mathrm{DIC}_{\mathrm{S}})\frac{p\mathrm{CO}_{2,\mathrm{pm}}}{\mathrm{DIC}_{\mathrm{pm}}}\ (\partial \ln p\mathrm{CO}_2/\partial \ln\mathrm{DIC})_{\mathrm{pm}} \tag{12}$$

When $\Delta p\mathrm{CO}_{2,\mathrm{bio}}$ is positive, respiration dominates over primary production. The changes in DIC due to air-sea exchange ($\Delta\mathrm{DIC}_{\mathrm{asf}}$) between observations were estimated from the air-sea flux as outlined in equation (9) without the recalculation to $p\mathrm{CO}_2$ (equation (13)):

$$\Delta\mathrm{DIC}_{\mathrm{asf}} = \frac{\int_{t_{\mathrm{pm}}}^{t_m} \mathrm{F}_{\mathrm{asf}}\mathrm{d}t}{h_{\mathrm{BD}}} \tag{13}$$

The impact of changes in salinity on DIC ($\Delta\mathrm{DIC}_{\mathrm{S}}$) was calculated using equation (8b). Note that the maximum effect of biological activity on TA is in the order of the maximum change in the NO_3^- concentration (e.g., ~10 μmol/kg over the phytoplankton bloom period). For that reason, the resultant effect on $p\mathrm{CO}_2$ was ignored.

To clarify seasonal patterns monthly changes in $p\mathrm{CO}_2$ due to thermal forcing, changes in salinity, mixing/advection, air-sea CO_2 fluxes, and biological forcing were estimated. The parameters were interpolated at the turns of the months, and changes between observations and/or turns of the months were calculated as described above and subsequently summed within months.

2.4. Error Propagation in the Calculated Effects of the Drivers on Surface Water $p\mathrm{CO}_2$

A Monte Carlo approach was used to estimate the propagated errors according to the following steps:

1. Normally distributed artificial random errors (n = 10,000) with a mean of zero and a standard deviation determined by the uncertainty of each property were added to the properties, respectively. The uncertainty is here the combined error that results from the accuracy and resolution/precision of the specific method used to determine the specific property. The documented resolution and accuracy of the CTD data are given in Appendix A (see Table A2). The precision and accuracy of TA is also given in Appendix A (see Table A2). For DIC and $p\mathrm{CO}_2$ the uncertainty refers to the error estimate that is outlined in section 2.3. The uncertainty in the flux is also estimated from the uncertainties outlined in section 2.3 and can be regarded as a lower bound of the real uncertainty. The uncertainty in the temperature coefficient is difficult to assess but was set to ±0.003 as a sensitivity test. This is roughly the difference between the temperature coefficients in Table 1 and the coefficient of Takahashi et al. (1993), which means that the coefficients in Table 1 result in 3‰ larger changes in $p\mathrm{CO}_2$ per degree Celsius. The uncertainties in the $\Delta\mathrm{TA}/\Delta S$ and $\Delta\mathrm{DIC}/\Delta S$ ratios were set to 2.5 μmol/kg per 1‰ to reflect the 4% difference between the $\Delta\mathrm{TA}/\Delta S$ ratio and the linear relationship in Figure 2a. The uncertainty in the calculated h_{BD} was estimated by a separate Monte Carlo approach to be around ±1 m, but the main uncertainty is of course the use of h_{BD} as an approximation of the depth over which a loss or gain in CO_2 is distributed. To give a number to this uncertainty the median relationship between the ratio of h_{BD} and the depth to which wind-driven turbulent mixing reaches (h_ε) and wind work was used (Randelhoff et al., 2017, see Figure 8b). On a monthly scale the wind work in Adventfjorden is high enough for the median ratio of h_{BD} and h_ε to vary between 1 and 1.5. For that reason the ratio of 1.25 was chosen and the uncertainty in h_{BD} was approximated from the differences between all estimates of h_{BD} and $h_{\mathrm{BD}}/1.25$, that is, in average 6 m, which gives an uncertainty of ±6 m. Note that for the iterations where h_{BD} (that ranged between 10 and 51 m)

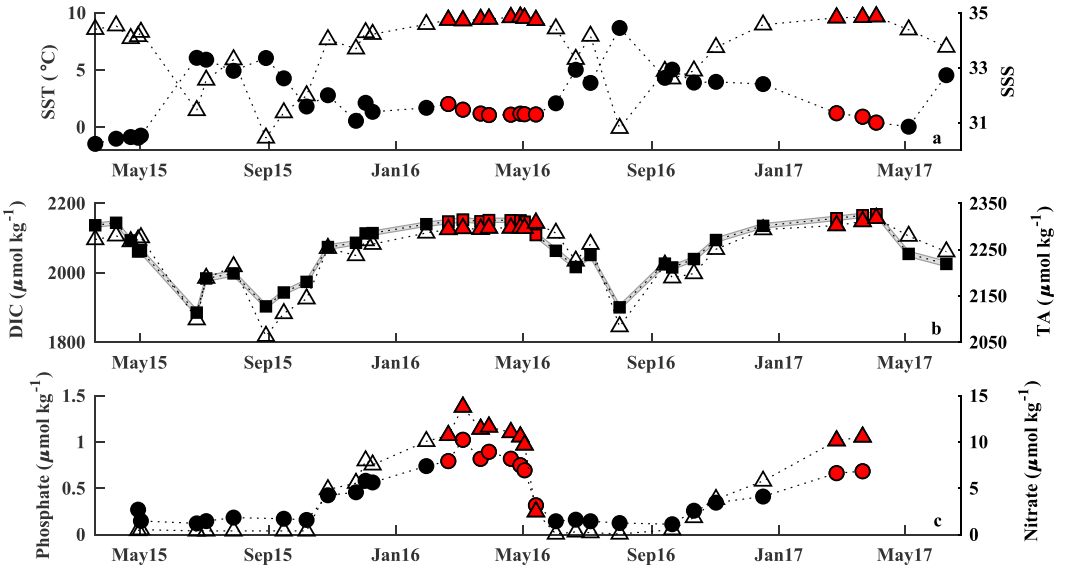

Figure 3. Time series of (a) sea surface temperature (SST, °C; dot) and sea surface salinity (SSS, open triangle), (b) total dissolved inorganic carbon (DIC, μmol/kg; filled square) with its associated estimated uncertainty (gray shade) and total alkalinity (TA, μmol/kg; open triangle), and (c) phosphate (μmol/kg; dot) and nitrate (μmol/kg; open triangle) concentrations. Red markers indicate the presence of Transformed Atlantic Water/Atlantic Water.

plus the random error were below 2 m, the sum was adjusted to 2 m to remove negative or close to zero values. This also reflects the depth from which reliable CTD measurements exist.

2. The properties plus the random errors were used to estimate $\Delta pCO_{2,T}$, $\Delta pCO_{2,S}$, $\Delta pCO_{2,mix,adv}$, $\Delta pCO_{2,asf}$, and $\Delta pCO_{2,bio}$ according to section 2.3, that is, 10,000 estimates for each term.
3. The standard deviation of the 10,000 estimates for each term was used as measure of the uncertainty.

3. Results

3.1. Hydrographic Conditions

The time series of the different parameters are shown in Figure 3. Between March 2015 and June 2017 the seasonal difference between winter and summer in SST at the IsA Station (Figure 3a) was around 7°C, that is, the maximum difference for each year, with the coldest conditions (−1.5°C) observed at the onset of the study. The two following winters were considerably warmer with temperatures averaging around 2°C. The highest observed values were 6.1°C in June 2015 and 8.7°C in August 2016, but the variability was considerably higher over the second summer.

In 2015 and early 2016 wintertime SSS was typically less than 34.6 (Figure 3a). This rather fresh water mass (ArW) was replaced in February 2016 by TAW that was also present the following winter. In June, regardless of year, SSS dropped below 34 and reached values below 31 in August. The impact of the freshening of the surface layer over the summer season was evident in the SSS throughout autumn.

The surface TA was around 2270 μmol/kg in spring 2015 and early winter 2016 (Figure 3b). These values increased to about 2,300 when TAW entered the site in February 2016. Similarly as for SSS, the addition of freshwater in the summer diluted TA with surface concentrations reaching minima of around 2,060–2,090 μmol/kg at the end of summer.

Surface DIC concentrations largely followed the observed seasonal patterns in SSS and TA, except for the drawdown of DIC that occurred in April–May before the onset of the melt season as seen in Figure 3b. Between January and April prebloom DIC concentrations reached values of around 2,140–2,170 μmol/kg with the highest values seen in 2017. The TAW had typically ~10–20 μmol/kg higher values than the fresher water mass that was observed in 2015 and early 2016. Summertime DIC concentrations dropped to around 1,900 μmol/kg in August, but the altogether lowest observed concentration (1,885 μmol/kg) was observed in June 2015.

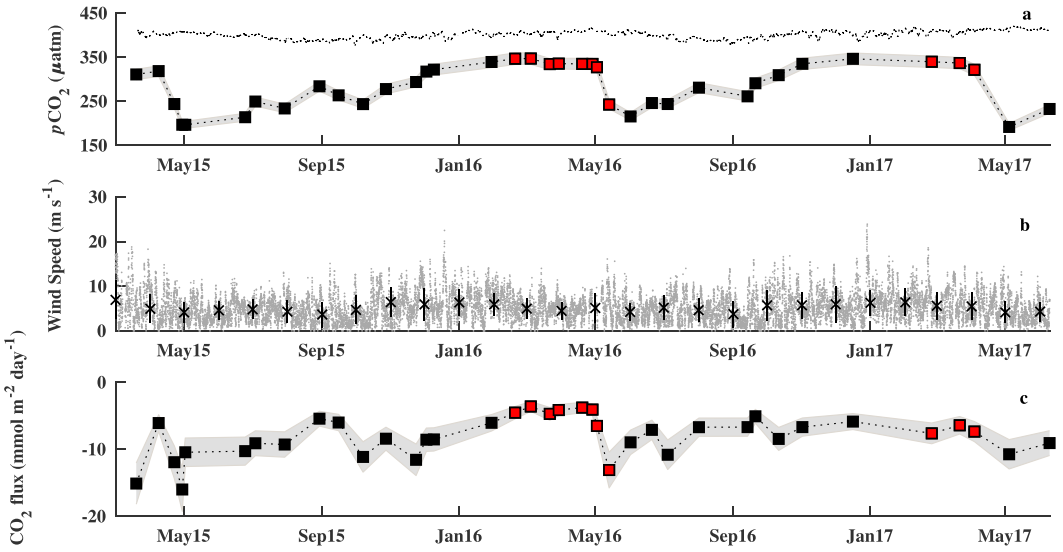

Figure 4. Time series of (a) calculated pCO_2 in air according to equation (4) for the air and vapor pressure at Longyearbyen airport using xCO_2 data from the Zeppelin mountain (hourly average, μatm; dotted black line), calculated pCO_2 in the surface water (μatm; black squares and uncertainty as indicated by gray shade), (b) hourly wind speed (m/s; gray dots) and monthly mean wind speed (m/s; black crosses with standard deviation), and (c) air-sea CO_2 flux (mmol·m^{-2}·day^{-1}; black squares and uncertainty as indicated by gray shade). Red markers indicate the presence of Transformed Atlantic Water/ Atlantic Water.

The nutrient data only extends between end of April in 2015 and March 2017 (Figure 3c). The surface concentrations of NO_3^- dropped sharply in midspring and remained close to the detection limit throughout the summer season. Late winter concentrations typically reached values of ~11 μmol/kg. PO_4^- concentrations varied from ~0.1 to 1 μmol/kg in the surface waters, following the trends observed in NO_3^-.

3.2. Surface Water pCO_2 and Air-Sea CO_2 Exchange

Between January and March pCO_2 varied from 310 to 350 μatm with higher values in 2016 and 2017 (Figure 4a). In April 2015, May 2016, and April 2017, the seawater pCO_2 dropped from the winter values mentioned above to around 200–250 μatm. These minima in pCO_2 that were more pronounced in 2015 and 2017 also coincided with low nutrient concentrations (around the detection limit for NO_3^- and 0.1–0.3 μmol/kg for PO_4^{3-}, Figure 3c). The surface water pCO_2 increased slowly over the summer and autumn months to reach winter values by the end of the year.

Atmospheric pCO_2 (Figure 4a) showed a less pronounced seasonal signal with summertime values from 380 to 395 to winter values between 400 and 415 μatm. The pCO_2 in the surface water was thereby undersaturated in CO_2 in relation to atmospheric CO_2 all year round with an air-sea pCO_2 gradient ranging between −51 and −217 μatm.

The monthly mean wind speed varied from 3.7 to 6.9 m/s (Figure 4b). The wind speed was slightly higher over the winter months compared to the summer season. The maximum wind speed of 26.5 m/s occurred during a storm event at the end of 2015, when the anemometer failed to log for a couple of hours due to the wind force.

The air-sea CO_2 fluxes varied between −4 and −16 mmol C·m^{-2}·day^{-1} (Figure 4c, negative values mean ocean CO_2 uptake), largely following the variability in surface water pCO_2; that is, the largest fluxes occurred generally when the surface water pCO_2 was at its minimum. Months with higher mean wind speed also contributed to high fluxes such as that observed in March 2015. The integrated annual fluxes were −35.8 ± 1.7 and −31.2 ± 1.8 g C·m^{-2}·year^{-1}, for the first and second annual cycles, respectively, beginning with the month of April.

3.3. Drivers of pCO_2 Variability

The different processes that drive changes in pCO_2 were investigated in terms of monthly changes following two full annual cycles, as estimated from the month of April (Figure 5). Primary production was responsible

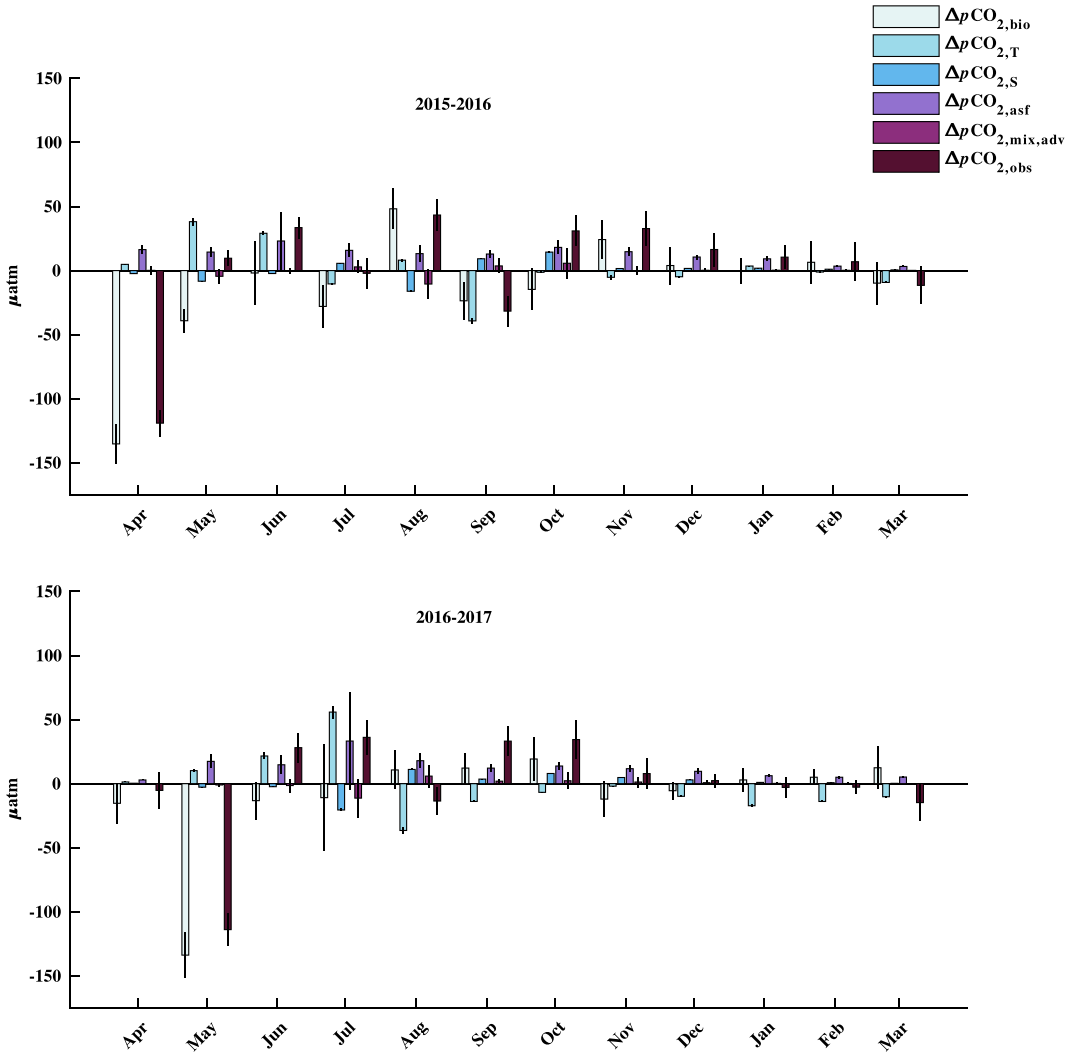

Figure 5. Monthly changes in pCO_2 (µatm) either observed ($\Delta pCO_{2,obs}$) or calculated from changes in biological activity (respiration and/or primary production, $\Delta pCO_{2,bio}$), temperature ($\Delta pCO_{2,T}$), salinity ($\Delta pCO_{2,S}$), air-sea flux ($\Delta pCO_{2,asf}$), and mixing/advection ($\Delta pCO_{2,mix,adv}$). Note that there exist no observations for the month of January in 2017. The uncertainty (black error bars) was calculated as outlined in section 2.4.

for a drop in pCO_2 of around 130–140 µatm in April 2015 and May 2016. This decrease was partly counteracted by the effect of warming, which contributed to a pCO_2 increase of ~70 µatm in May and June 2015 and nearly 90 µatm between May and July in 2016. The effect of warming was followed by cooling in late summer and autumn which decreased pCO_2. The maximum monthly changes in pCO_2 due to decreased salinity over the melt season were in the order of 20 µatm as observed in August 2015 and July 2016, which was counteracted by increases in salinity toward autumn. The magnitude of the combined effect of mixing and advection on pCO_2 was in the order of 0.1 to 10 µatm on a monthly scale. The monthly effect of air-sea CO_2 fluxes on pCO_2 was strongest in the summer months, for example, 21 µatm in June 2015 and 26 µatm in July and August 2016, when the stratification of the surface layer was more pronounced.

Between December and March, $\Delta pCO_{2,bio}$ was in average 2 ± 7 µatm. Similarly, $\Delta pCO_{2,T}$, $\Delta pCO_{2,S}$, $\Delta pCO_{2,mix,adv}$, $\Delta pCO_{2,asf}$, and $\Delta pCO_{2,obs}$ were in average −8 ± 7, 1 ± 1, 0.3 ± 0.2, 7 ± 3, and 1 ± 11 µatm, which suggests that the variation in pCO_2 and the effects of its associated drivers are small in the winter season.

On an annual scale, the biological processes resulted in a net decrease in pCO_2 of 170 and 128 µatm over the first and second annual cycles, respectively (Table 2), but the uncertainties in these estimates are large. Still,

Table 2
Net Annual Change in Surface Water pCO_2 (μatm) at the IsA Station Between April 2015, 2016, and 2017

Period	$\Delta pCO_{2,bio}$	$\Delta pCO_{2,T}$	$\Delta pCO_{2,S}$	$\Delta pCO_{2,asf}$	$\Delta pCO_{2,mix,adv}$	$\Delta pCO_{2,obs}$
2015–2016	−170 ± 37	12 ± 5	7 ± 1	155 ± 28	−2 ± 22	20 ± 14
2016–2017	−128 ± 50	−21 ± 7	7 ± 1	150 ± 43	−1 ± 21	−11 ± 15

Note. The annual changes were estimated from the observed changes ($\Delta pCO_{2,obs}$) as well as from the monthly changes outlined in section 2.3, that is, changes in biological activity ($\Delta pCO_{2,bio}$), temperature ($\Delta pCO_{2,T}$), salinity ($\Delta pCO_{2,S}$), air-sea flux ($\Delta pCO_{2,asf}$), and mixing/advection ($\Delta pCO_{2,mix,adv}$).

the net effect was negative and the annual effect of primary production on surface water pCO_2 largely exceeds the effect of respiration. The net effect of biological activity (primary production) was counteracted by air-sea CO_2 exchange that resulted in a net increase in pCO_2 of around 150 μatm for both years. The effects of temperature and salinity on surface water pCO_2 were an order of magnitude smaller. The net effect of salinity was positive over both annual cycles resulting in an increase of pCO_2 of 7 μatm for each year. The net impact of temperature on the other hand was positive over the first annual cycle by the end of which warm TAW had entered the site and negative the following year. Mixing and advection had a minimal impact on pCO_2 on an annual scale.

The relative contribution of biological activity to the total change in pCO_2, as estimated from the annual sum of the absolute valued changes, was 41% and 32% for the first and second annual cycles, respectively (Figure 6). Temperature, on the other hand, contributed with 19% and 25% of the total change in pCO_2 over the first and second annual cycles, respectively. The air-sea flux accounted for 19% of the total change. The contribution of salinity, in terms of the solubility effect on pCO_2, to the total change (7–8%) was smaller in size compared to the residual term (9–13%), but twice as large as the contribution of mixing and advection (3–4%).

4. Discussion

4.1. Variability of Air-Sea CO_2 Exchange

Spitsbergen is situated at the borders of the central Arctic Ocean and the Barents Sea and surrounded by surface waters with documented low seawater pCO_2 compared to the atmosphere (e.g., Fransson et al., 2017; Lauvset et al., 2013; Yasunaka et al., 2016). This is also the case for the IsA Station in Adventfjorden where the surface waters were undersatured in CO_2 compared to the atmosphere all year round and the air-sea pCO_2 gradient ranged between −51 and −217 μatm.

These values can be compared to air-sea pCO_2 gradients in March and September of around −30 to −140 μatm in the nearby glacial influenced fjord branch of Isfjorden, Tempelfjorden (Fransson et al., 2015), and in April and July of −70 to −200 μatm in Kongsfjorden further north (Fransson et al., 2016). The uptake potential, based on the air-sea pCO_2 gradient in these fjords, should therefore be close to comparable to that of Adventfjorden. As an example, the September air-sea pCO_2 gradient in Tempelfjorden of close to −130 to −140 μatm (Fransson et al., 2015), with SST and SSS of around 3°C and 32.2, respectively, results in fluxes of −6.3 to −6.8 mmol C·m^{-2}·day^{-1}, when using the September mean squared wind speed of 22.5 m^2/s^2 at Longyearbyen airport. These values are comparable to the calculated September fluxes at the IsA Station of −5.1 to −6.7 mmol C·m^{-2}·day^{-1} (Figure 4). However, the actual uptake in Tempelfjorden, as well as in Kongsfjorden, will be a result of the local wind distribution and on a yearly basis the length of the ice-free period will play a significant role.

Shifting the focus from the West Spitsbergen fjord systems to the surrounding areas, Fransson et al. (2017) observed air-sea pCO_2 gradients in January to June of −81 to −254 μatm (including sea ice) in the surface waters north of Svalbard (on the slope and in the Nansen Basin) and Omar et al. (2007) and Lauvset et al. (2013) give monthly mean estimates for the neighboring productive Barents Sea ranging between −10 and −100 μatm. Although comparable pCO_2 gradients, the annual CO_2 uptake rates of 31–36 g C·m^{-2}·year^{-1} found for the IsA Station are smaller than the uptake rates estimated for waters north of Svalbard (potential ice-free uptake: ~44–114 g C·m^{-2}·year^{-1}, Fransson et al., 2017) as well as for waters in the Barents Sea (46 g C·m^{-2}·year^{-1}, Nakaoka et al., 2006; 51 g C·m^{-2}·year^{-1}, Omar et al., 2007;

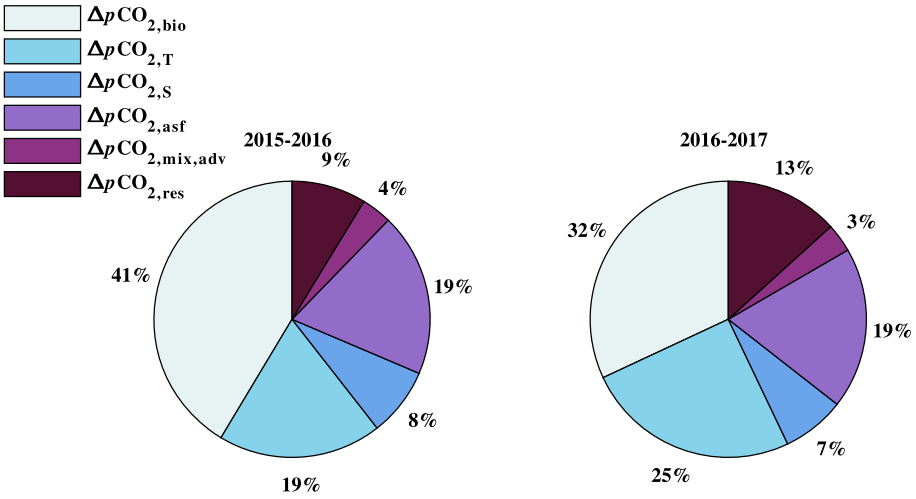

Figure 6. Pie chart over the annual sum of absolute valued monthly changes in pCO_2 due to biological activity, temperature, salinity, air-sea exchange, mixing/advection, and the residual ($\Delta pCO_{2,res}$). The latter is the change that remains when the effects of the other processes are withdrawn from the observed change.

48 g C·m^{-2}·year^{-1}, Lauvset et al., 2013; ~44 g C·m^{-2}·year^{-1}, Yasunaka et al., 2016), with a few exceptions (e.g., Land et al., 2013; Takahashi et al., 2009).

One possible reason for the observed differences in uptake rates between Adventfjorden (31–36 g C·m^{-2}·year^{-1}) and the neighboring regions (44–114 g C·m^{-2}·year^{-1}) is the gas transfer velocity both in terms of the wind speed parameterization as well as of the wind speed distribution. The estimated rates of Fransson et al. (2017) are based on comparable methods, but the studies from the Barents Sea differ from the present study. Nakaoka et al. (2006) did not specifically state which wind speed relationship their flux estimates were based on, but Lauvset et al. (2013) and Omar et al. (2007) used the wind speed relationships of Wanninkhof (1992) for long-term averaged winds of a year or more and short-term averaged winds, respectively. The latter suffered from its assumption of a Rayleigh distribution of the wind speed. Applying the two wind speed relationships for comparison to the data set from the IsA Station would increase or decrease the estimated uptake rates by around 16% for the long-term and short-term formulas, respectively. Yasunaka et al. (2016) rescaled the gas transfer coefficient of Sweeney et al. (2007) of 0.27 to 0.19 to fit the U.S. National Centers for Environmental Prediction-Department of Energy Reanalysis 2 wind speed product (NCEP-2), which applied to the present data set also would reduce the uptake rates. None of these comparisons are straightforward because of the local scale of the present study as well as the use of different wind products.

Since the different wind speed formulas did not resolve the observed differences in uptake rates between Adventfjorden and the Barents Sea, the wind speed distribution must play an important part. As an example of that, the wind speed distribution at Svalbard Airport over the first annual cycle is shown in Figure 7 together with the NCEP-2 wind distribution. The wind speed data subset for the Isfjorden region (77–79°N, 13–19°E) was provided by the NOAA/OAR/ESRL PSD, Boulder, Colorado, United States (https://www.esrl.noaa.gov/psd/data/gridded/data.ncep.reanalysis2.pressure.html). The frequency at higher wind speeds quickly drops to close to zero at Longyearbyen airport, as opposed to the more large-scale NCEP-2 wind speeds. This difference, apart from the uncertainty in the NCEP-2 product, could be a result of the local impact of the mountains that surrounds Adventfjorden and/or reflect a bias in the measured winds due to the location of the wind meter. Using an annual mean air-sea pCO_2 gradient of −108 μatm for the IsA Station and a gas transfer velocity estimated from the squared NCEP-2 wind speed and the wind speed relationship used by Yasunaka et al. (2016), the estimated annual uptake at the IsA Station would then be higher, around 57 g C·m^{-2}·year^{-1}. This implies that the surface waters of Adventfjorden have the potential to be a strong sink for atmospheric CO_2 as long as the wind distribution allows an efficient gas transfer.

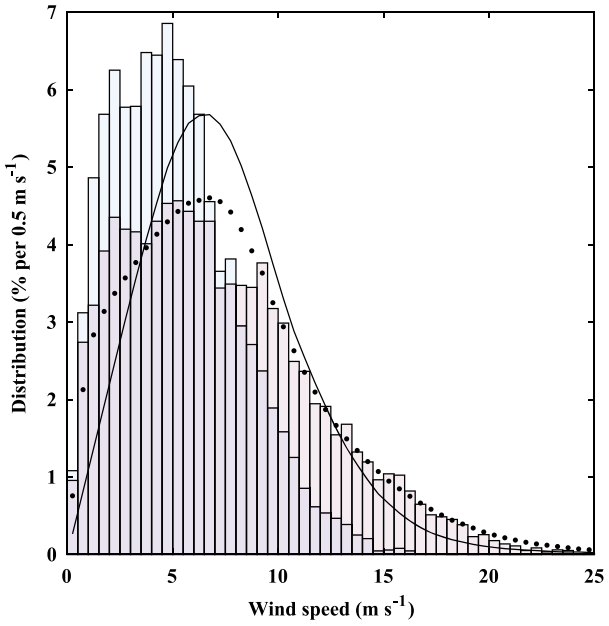

Figure 7. Histogram of the distribution of winds at Svalbard Airport (pale blue bars), and NCEP-2 over the Isfjorden area (77–79°N, 13–19°E, with a resolution of 2 ×2, pale purple bars) for the period 1 April 2015 to 1 April 2016. Solid line is the global Cross-Calibrated Multi-Platform distribution, and the dotted line is the global NCEP-2 distribution for 1990–2009 (Wanninkhof, 2014). NCEP-2 = U.S. National Centers for Environmental Prediction-Department of Energy Reanalysis 2 wind speed product.

With this in mind, the comparisons will now be extended to the glacier-influenced Greenland fjords. These studies have typically used the gas transfer velocity formula of Nightingale et al. (2000), which is comparable to that of Wanninkhof (2014) within a few percentages. Also here, the integrated uptake rates of 31–36 g C·m^{-2}·year^{-1} at the IsA Station fall in the lower range (32 g C·m^{-2}·year^{-1}, Sejr et al., 2011; 19–172 g C·m^{-2}·year^{-1}, Rysgaard et al., 2012; 37–70 g C·m^{-2}·year^{-1}, Meire et al., 2015). The estimated uptake of Sejr et al. (2011) was conducted in Young Sound and is based on a mean July–August air-sea pCO_2 gradient of −106 μatm over the sea ice-free period (94 days). This can be compared to annually integrated mean air-sea pCO_2 gradients at the IsA Station of −100 to −120 μatm. Considering that the air-sea pCO_2 gradients are comparable and the overall short period of air-sea gas exchange in Young Sound due to the extensive sea ice cover, the high annual uptake of 32 g C·m^{-2}·year^{-1} (that includes an ice formation period of 10 days with an efflux of 1.1 mmol·m^{-2}·day^{-1}) must be a result of more intense winds compared to the situation in Adventfjorden. The uptake rates in the Godthåbsfjord SW Greenland showed considerable interannual variability and the maximum annual uptake rate was more than 150 g C·m^{-2}·year^{-1} higher than the lowest (Rysgaard et al., 2012). This reflects a large interannual variability in the monthly air-sea pCO_2 gradient that ranged between −350 and 350 μatm over the whole study, but there was also interannual variability in the monthly mean wind speed. In contrast, the two annual cycles of CO_2 uptake in Adventfjorden differed with as little as 5 g C·m^{-2}·year^{-1} despite the observed shift between Arctic to Atlantic origin waters (Figure 4).

Recent changes in the atmospheric circulation (Isaksen et al., 2016) have been suggested to facilitate the intrusion of Atlantic Water onto the shelf as well as into the West Spitsbergen fjords (Nilsen et al., 2016). The difference in the CO_2 uptake rates between Arctic and Atlantic origin waters were evaluated, with the awareness that 2 years of observations are unlikely to capture the overall natural variability in the air-sea CO_2 fluxes. Prebloom and winter fluxes from March, April, and December in 2015 (Arctic conditions) were compared to prebloom values from February to April in 2016 when TAW dominated the water column ($n_{2015} = n_{2016} = 4$). The mean squared wind speed and mean atmospheric pCO_2 over the mentioned months (40.8 m^2/s^2 and 404 μatm, respectively) were used in the comparison. The fluxes of the Arctic origin waters were significantly higher and the surface water pCO_2 was significantly lower (2 mmol C·m^{-2}·day^{-1} and 24 μatm, respectively, $p = 0.001$ for both tests), as compared to those of the TAW. If the investigated periods are representative for the two water masses, especially considering that the West Spitsbergen fjords are going through some major transitions (a reduction in the sea ice cover, Muckenhuber et al., 2016; a warming of the Atlantic Water of 0.2°C per decade in Isfjorden, Pavlov et al., 2013), and if the atmospheric forcing continues to transport Atlantic Water into the fjord systems, the CO_2 uptake capacity could decrease in this region.

4.2. Impact of Drivers on pCO_2

Biological processes in terms of primary production and respiration together with temperature were the two main drivers that control surface water pCO_2 in Adventfjorden on a monthly scale (Figures 5 and 6). To validate the importance of biological processes and temperature effects on pCO_2, surface water pCO_2 was also modeled as a function of different combinations of T, S, NO_3^- using multiple linear regression (MLR) relationships (Appendix B). The linear combinations of T, S, and NO_3^- reflect not only the thermodynamic dependencies of seawater pCO_2 on T and S (e.g., Takahashi et al., 1993) but also the effects of primary production and remineralization through the Redfield stoichiometric relationship between NO_3^- and DIC (e.g., Redfield et al., 1963; Sarmiento & Gruber, 2006), which translates to changes in pCO_2. Although it should be noted that nutrients also vary to some extent due to mixing, NO_3^- and temperature had the highest predictive power of seawater pCO_2 ($R_{adj}^2 = 0.8$, Table B1).

Biological activity was likewise a key driver for surface water pCO_2 on an annual scale together with air-sea exchange that essentially counteracts the effect of primary production in spring (Table 2). The importance for biological CO_2 consumption has also been observed in the waters north of Svalbard (January–June), with a relative effect of 26% (Fransson et al., 2017), as compared to the 32–41% in Adventfjorden.

Temperature is, typically together with biological processes, a key driver of pCO_2 variability in the Global Ocean, for example, such as observed in the North Atlantic by Lüger et al. (2004), or in the subarctic North Pacific Ocean (Chierici et al., 2006), but temperature is not necessarily important in the Arctic Ocean (Chierici et al., 2011). One reason to why temperature is important in Adventfjorden could be the current lack of sea ice in large parts of the Isfjorden system (Muckenhuber et al., 2016). The lack of ice not only allows a continuous air-sea heat and gas exchange, but it also removes the impacts of different sea ice processes that may affect the surface water pCO_2. For instance, in waters north of Svalbard the relative effect of the total change in seawater fCO_2 (or pCO_2) as a result of $CaCO_3$ (ikaite) dissolution was estimated to 38% over the winter-spring period (Fransson et al., 2017).

Salinity had only a small relative effect of 7–8% on the surface water pCO_2 at the IsA Station, which reflects the rather modest seasonal difference of around 4 between winter and late summer. In comparison, the SSS drops to around 20 in the Greenland fjords (Meire et al., 2015; Rysgaard et al., 2012; Sejr et al., 2011). Meire et al. (2015) estimated that the release of glacial meltwater in the Godthåbsfjord accounted for as much as 28% of the CO_2 uptake.

So far, the discussion has ignored the effects of riverine input of nutrients and organic matter on surface water pCO_2. The main reason for this is the rather small impacts these riverine constituents have on the pCO_2 variability at the outer part of Adventfjorden. First, Wynn et al. (2007) observed NO_3^- concentrations in glacial runoff of $\leq$5 μmol/L (Midtre Lovénbreen, Ny Ålesund, Spitsbergen). For a maximum freshwater fraction (f_{fw}) of 12% as estimated from equation (14):

$$f_{fw} = \frac{S_{\text{winter}} - S}{S_{\text{winter}}} \tag{14}$$

where S = 30.4 (minimum salinity observed on 29 August 2015) and a winter reference salinity (S_{winter}) of 34.7, a meltwater NO_3^- concentration of 5 μmol/L would increase the seawater NO_3^- concentration by 0.6 μmol/L, which corresponds to 0.2 $\mu mol \cdot L^{-1} \cdot month^{-1}$ over the melt season. If this added NO_3^- was fixated into organic matter the corresponding decrease in DIC would be 1 $\mu mol \cdot L^{-1} \cdot month^{-1}$, for a classical stoichiometric Redfield ratio between carbon and nitrogen (C/N) of 6.6 (Redfield et al., 1963). The effect on surface water pCO_2 would not be discernible. Second, the riverine input of organic matter has little impact on the surface water pCO_2 since the concentration of NO_3^- remains close to the detection limit throughout the summer season ($NO_3^- < 0.4$ μmol/L). That means that any decay products of riverine organic matter will be absorbed and fixated into new organic matter with the net effect on surface water pCO_2 being zero.

5. Conclusion

Adventfjorden, similar to surrounding polar and subpolar regions, is a net annual CO_2 sink. The uptake potential, in terms of the air-sea pCO_2 gradient, is close to similar to neighboring fjords of the West Spitsbergen, to ice-covered waters north of Svalbard, and to the surface waters of the Barents Sea. The wind distribution over the fjord, as estimated from the wind meter at Svalbard Airport, is, however, shifted toward lower wind speeds. The result is a more modest annual uptake rate (31–36 g $C \cdot m^{-2} \cdot year^{-1}$) compared to most estimates in the surrounding areas.

The fluxes were significantly higher in the Arctic origin waters compared to fluxes of TAW. If Atlantic Water continues to be transported into the West Spitsbergen fjords over the coming years, as observed over recent years (Pavlov et al., 2013), the CO_2 uptake capacity could be diminished in this area. On the other hand, if the observed warming of the Atlantic Water of the West Spitsbergen Current (e.g., 0.2°C per decade, Isfjorden, Pavlov et al., 2013; 0.3°C per decade north of Svalbard, Onarheim et al., 2014) also continues, this could possibly result in an increased amount of glacial meltwater being released to the fjords. The outcome of these

potential warming and freshening effects on surface pCO_2 needs to be further evaluated. So far, on a seasonal scale, the main drivers for the observed pCO_2 variability are biological processes and to a lesser extent temperature, which likely reflect the current ice-free conditions at the IsA Station, but this may change in the coming future of climate change.

Appendix A: Data Provenance

An overview of the sampling occasions, including the CTD-devices that were used and the discrete water samples that were collected, is presented in Table A1. The documented accuracy and resolution of the different CTD-instruments are given in Table A2, together with uncertainties in the input parameters (i.e. TA, pH, T, K1 and K2) that were used in the CO2SYS software to calculate pCO_2 and DIC.

Table A1
Data Overview

Dates	CTD	Samples	TA/pH	Nutrients
19 March 2015	SD204	4	Yes	NA
8 April 2015	SD 204	8	Yes	NA
22 April 2015	SBE19+[a]	8	Yes	NA
29 April 2015	SD204	8	Yes	Yes
2 May 2015	SBE9	5	Yes	Yes
24 June 2015	SD204	8	Yes	Yes
3 July 2015	SD204	8	Yes	Yes
29 July 2015	SBE37	8	Yes	Yes
29 August 2015	SBE9	5	Yes[b]	NA
15 September 2015	SD204	5	Yes	Yes
7 October 2015	SD204	5	Yes	Yes
27 October 2015	SBE37	5	Yes	Yes
23 Nov 2015	SBE37	8	Yes	Yes
2 December 2015	SBE37	5	Yes	Yes
9 December 2015	SBE37[c]	8	Yes	Yes
29 January 2016	SBE37	5	Yes	Yes
19 February 2016	SBE19+	5	Yes	Yes
4 March 2016	SBE19+	5	Yes	Yes
21 March 2016	SBE19+	5	Yes	Yes
29 March 2016	SBE19+	5	Yes	Yes
19 April 2016	SBE19+	5	Yes	Yes
28 April 2016	SD204[d]	8	Yes	Yes
2 May 2016	SBE19+	8	Yes	Yes
13 May 2016	SBE19+	5	Yes	Yes
1 June 2016	SBE19+	5	Yes	Yes
20 June 2016	SBE19+	5	Yes	Yes
4 July 2016	SBE19+	5	Yes	Yes
1 August 2016	SBE19+	5	Yes	Yes
13 September 2016	SBE9	7	Yes[e]	NA
20 September 2016	SD204[f]	5	Yes	Yes
11 October 2016	SBE19+	5	Yes	Yes
1 November 2016	SBE19+	5	Yes	Yes
16 December 2016	SBE19+	5	Yes	Yes
24 February 2017	SD204[g]	5	Yes	Yes
21 March 2017	SD204[g]	5	Yes	Yes
3 April 2017	SD204[g]	5	Yes	NA
4 May 2017	SBE19+	5	Yes	NA
9 June 2017	SBE19+	5	Yes	NA

Note. CTD = conductivity-temperature-depth; TA = total alkalinity; NA = not applicable.
[a]Measurements were conducted 17 April 2015. [b]Fixated with $HgCl_2$ and analyzed within 6 weeks. [c]Measurements were conducted 10 December 2015. [d]Salinity corrected for an offset of −0.10. [e]Analyzed 2 days after sampling. [f]Noise in pressure measurements; i.e., pressure was modeled, salinity recalculated for the new pressure, and finally, salinity was corrected for an offset of −0.13. [g]Salinity corrected for an offset of −0.14.

Table A2
Uncertainties in Parameters Used to Calculate the Marine CO_2 System, Air-Sea CO_2 Fluxes, and Effects of Drivers on Surface Water pCO_2

Parameters	Precision/*Resolution*	Accuracy
TA (μmol/kg)	±2(±4)[a]	±2(±4)
pH	±0.001[a]	±0.005
T (°C)[b]	0.1	±0.3
T (°C)[c]	0.001[1], 0.0001[2,4], 0.0002[3]	±0.01[1], ±0.005[2], ±0.001[3], ±0.002[4]
S[c]	0.01[1]	±0.02[1](±0.1[1])
C[c] (mS/cm)	0.0005[2], 0.0004[3], 0.0001[4]	±0.005[2], ±0.003[3,4]
K_1 (%)[d]	±2.5	
K_2 (%)[d]	±4.6	

Note. TA = total alkalinity.
[a]These values are the experimental precision reported as the mean absolute difference between duplicate sample runs, with the value for the endpoint determination in parentheses. [b]The laboratory temperature was measured using a digital probe (TFX410, technical data in the table), except for March to July 2015, and July and August 2016, when a flow-through thermistor was used. [c]Temperature, salinity, and conductivity (*C*) were obtained from the following conductivity-temperature-depth devices: (1) SD204, SAIV A/S, Norway (the value in brackets represents an offset that was corrected for as noted in Table A1), (2) SBE 19+, Seabird Electronics, United States, (3) SBE 9, Seabird Electronics, United States, and (4) SBE 37 MicroCAT, Seabird Electronics, United States. [d]These values are the experimental precision ($2S_f$).

Appendix B: Multiple Linear Regression Relationships

Paragraphs have already been provided for Appendix B. Only Appendix A needed them. Please ensure Appendix B is presented correctly.

pCO_2 was modeled as a function of different combinations of *T*, *S*, NO_3^-, and PO_4^{3-} using MLR relationships and a summary of selected results is shown in Table B1. The MLRs took the following form, for example,

$$pCO_2 = a_0 + a_1\left[NO_3^-\right] + a_2T + a_3S \quad \text{(B1)}$$

where a_0 through a_3 are the regression coefficients and the NO_3^- concentration was interchanged with the PO_4^{-3} concentration. The determination of the coefficients can be improved if the predictor variables are centered, that is, subtracting the mean from each property, but the aim here is rather to investigate the importance of the individual predictors. This goal was achieved by stepwise regressions where individual predictors were omitted to investigate the resultant change in the explained variation by the original model. The interaction terms were excluded from the models. The variance inflation factor was used to investigate collinearity between the predictor variables. The best combination of predictor variables was then chosen based on the variance inflation factor results and the R_{adj}^2 of the MLR relationship.

Table B1
Summary of Selected MLR Relationships of pCO_2 as a Function of [NO_3^-], SST, and SSS (n = 30)

Dependent variable	Predictor variables	VIF	Coefficients	SE	*p*	R_{adj}^2	RMSE
MLR							
pCO_2	Constant	1.9, 2.3, 3.3	173.6	221.8	0.44	0.796	± 22.7
	$[NO_3^-]$		10.8	1.2	$3.1{\cdot}10^{-9}$		
	SST		8.8	3.0	$6.1{\cdot}10^{-3}$		
	SSS		1.1	6.5	0.86		
pCO_2	Constant	1.4, 1.4	212.1	10.4	$5.8{\cdot}10^{-18}$	0.803	± 22.3
	$[NO_3^-]$		10.9	1.0	$2.7{\cdot}10^{-11}$		
	SST		8.5	2.2	$6.9{\cdot}10^{-4}$		
pCO_2	Constant	1.9, 1.9	620.2	186.1	$2.5{\cdot}10^{-3}$	0.736	± 25.8
	$[NO_3^-]$		10.9	1.4	$2.3{\cdot}10^{-8}$		
	SSS		−11.4	5.6	$5.3{\cdot}10^{-2}$		
SLR							
pCO_2	Constant		244.5	7.3	$4.6{\cdot}10^{-24}$	0.707	± 27.2
	$[NO_3^-]$		8.9	1.1	$3.6{\cdot}10^{-9}$		
$pCO_{2,T\,=\,2.4°C}$	Constant		227.7	5.5	$1.3{\cdot}10^{-26}$	0.887	± 20.4
	$[NO_3^-]$		12.0	0.8	$5.4{\cdot}10^{-15}$		

Note. SST = sea surface temperature; SSS = sea surface salinity; MLR = multiple linear regression; RMSE = root-mean-square error; SLR = simple linear regression.

Acknowledgments
The fieldwork was mainly funded by Arctic Field grant (RiS: 10127, 10404, and 10662), which is given by the Research Council of Norway, with additional support from course activities at the University Centre in Svalbard (UNIS). Metadata is available at the RiS portal at www.researchinsvalbard.no. Data will be available within a year after publication at the Norwegian Marine Data Centre (NMDC), until then contact the corresponding author. CO_2 atmospheric data are available from the EBAS database: http://ebas.nilu.no with annual updates. We thank especially M. Porcires and L.-F. Stangeland, and also the whole logistic department at UNIS, for technical and logistic support. We also thank the marine researchers at the Department of Arctic Biology at UNIS for collaboration and support with the fieldwork. The study was also supported by the Ocean Acidification flagship within the FRAM-High North Centre for Climate and the Environment, Norway (A. Fransson and M. Chierici). The atmospheric xCO_2 data were supported by the Norwegian Research Council project Signals from the Arctic Ocean in the Atmosphere-SOCA. Finally, we give thanks to the Norwegian Meteorological Institute for the data from Svalbard Airport.

References

Andersson, A., Falck, E., Sjöblom, A., Kljun, N., Sahlée, E., Omar, A. M., & Rutgersson, A. (2017). Air-sea gas transfer in high Arctic fjords. *Geophysical Research Letters*, *44*, 2519–2526. https://doi.org/10.1002/2016GL072373

Bates, N. R., & Mathis, J. T. (2009). The Arctic Ocean marine carbon cycle: Evaluation of air-sea CO_2 exchanges, ocean acidification impacts and potential feedbacks. *Biogeosciences*, *6*(11), 2433–2459. https://doi.org/10.5194/bg-6-2433-2009

Chen, B., Cai, W.-J., & Chen, L. (2015). The marine carbonate system of the Arctic Ocean: Assessment of internal consistency and sampling considerations, summer 2010. *Marine Chemistry*, *176*, 174–188. https://doi.org/10.1016/j.marchem.2015.09.007

Chierici, M., Fransson, A., & Anderson, L. G. (1999). Influence of *m*-cresol purple indicator additions on the pH of seawater samples: Correction factors evaluated from a chemical speciation model. *Marine Chemistry*, *65*(3-4), 281–290. https://doi.org/10.1016/S0304-4203(99)00020-1

Chierici, M., Fransson, A., Lansard, B., Miller, L. A., Mucci, A., Shadwick, E., et al. (2011). The impact of biogeochemical processes and environmental factors on the calcium carbonate saturation state in the Circumpolar Flaw Lead in the Amundsen Gulf, Arctic Ocean. *Journal of Geophysical Research*, *116*, C00G09. https://doi.org/10.1029/2011JC007184

Chierici, M., Fransson, A., & Nojiri, Y. (2006). Biogeochemical processes as drivers of surface fCO_2 in contrasting provinces in the subarctic North Pacific Ocean. *Global Biogeochemical Cycles*, *20*, GB1009. https://doi.org/10.1029/2004GB002356

Clayton, T. D., & Byrne, R. H. (1993). Spectrophotometric seawater pH measurements: Total hydrogen ion concentration scale calibration of m-cresol purple and at-sea results. *Deep Sea Research, Part I*, *40*(10), 2115–2129. https://doi.org/10.1016/0967-0637(93)90048-8

Cottier, F. R., Tverberg, V., Inall, M. E., Svendsen, H., Nilsen, F., & Griffiths, C. (2005). Water mass modification in an Arctic fjord through crossshelf exchange: The seasonal hydrography of Kongsfjorden, Svalbard. *Journal of Geophysical Research*, *110*, C12005. https://doi.org/10.1029/2004JC002757

Dickson, A. G. (1990). Standard potential of the reaction: AgCl (s) + $1/2H_2$ (g) = Ag (s) + HCl (aq), and the standard acidity constant of the ion HSO_4^- in synthetic sea water from 273.15 to 318.15 K. *The Journal of Chemical Thermodynamics*, *22*, 113–127. https://doi.org/10.1016/0021-9614(90)90074-Z

Dickson, A. G., & Millero, F. J. (1987). A comparison of the equilibrium constants for the dissociation of carbonic acid in seawater media. *Deep Sea Research Part A*, *34*(10), 1733–1743. https://doi.org/10.1016/0198-0149(87)90021-5

Department of Energy (1994). In A. G. Dickson, & C. Goyet (Eds.), *Handbook of methods for the determination of the parameters of the oceanic carbon dioxide system (version 2)*. Oak Ridge, Tennessee: ORNL/CDIAC-74, CDIAC.

Else, B. G. T., Galley, R. J., Lansard, B., Barber, D. G., Brown, K., Miller, L. A., et al. (2013). Further observations of a decreasing atmospheric CO_2 uptake capacity in the Canada Basin (Arctic Ocean) due to sea ice loss. *Geophysical Research Letters*, *40*, 1132–1137. https://doi.org/10.1002/grl.50268

Else, B. G. T., Papakyriakou, T. N., Galley, R. J., Mucci, A., Gosselin, M., Miller, L. A., et al. (2012). Annual cycles of pCO_{2sw} in the southeastern Beaufort Sea: New understandings of air–sea CO_2 exchange in Arctic polynya regions. *Journal of Geophysical Research*, *117*, C00G13. https://doi.org/10.1029/2011JC007346

Evans, W., Mathis, J. T., Cross, J. N., Bates, N. R., Frey, K. E., Else, B. G. T., et al. (2015). Sea-air CO_2 exchange in the western Arctic coastal ocean. *Global Biogeochemical Cycles*, *29*, 1190–1209. https://doi.org/10.1002/2015GB005153

Fransson, A., Chierici, M., Hop, H., Findlay, H. S., Kristiansen, S., & Wold, A. (2016). Late winter-to-summer change in ocean acidification state in Kongsfjorden, with implications for calcifying organisms. *Polar Biology*, *39*(10), 1841–1857. https://doi.org/10.1007/s00300-016-1955-5

Fransson, A., Chierici, M., Miller, L. A., Carnat, G., Shadwick, E., Thomas, H., et al. (2013). Impact of sea-ice processes on the carbonate system and ocean acidification at the ice-water interface of the Amundsen Gulf, Arctic Ocean. *Journal of Geophysical Research: Oceans*, *118*, 7001–7023. https://doi.org/10.1002/2013JC009164

Fransson, A., Chierici, M., Nomura, D., Granskog, M. A., Kristiansen, S., Martma, T., & Nehrke, G. (2015). Effect of glacial drainage water on the CO_2 system and ocean acidification state in an Arctic tidewater-glacier fjord during two contrasting years. *Journal of Geophysical Research: Oceans*, *120*. https://doi.org/10.1002/2014JC010320, 2413–2429.

Fransson, A., Chierici, M., Skjelvan, I., Olsen, A., Assmy, P., Peterson, A. K., et al. (2017). Effects of sea-ice and biogeochemical processes and storms on under-ice water fCO_2 during the winter-spring transition in the high Arctic Ocean: Implications for sea-air CO_2 fluxes. *Journal of Geophysical Research: Oceans*, *122*, 5566–5587. https://doi.org/10.1002/2016JC012478

Isaksen, K., Nordli, Ø., Førland, E. J., Lupikasza, E., Eastwood, S., & Niedźwiedź, T. (2016). Recent warming on Spitsbergen—Influence of the atmospheric circulation and sea ice cover. *Journal of Geophysical Research: Atmospheres*, *121*, 11,913–11,931. https://doi.org/10.1002/2016JD025606

Jutterström, S., & Anderson, L. G. (2010). Uptake of CO_2 by the Arctic Ocean in a changing climate. *Marine Chemistry*, *122*(1-4), 96–104. https://doi.org/10.1016/j.marchem.2010.07.002

Land, P. E., Shutler, J. D., Cowling, R. D., Woolf, D. K., Walker, P., Findlay, H. S., et al. (2013). Climate change impacts on sea-air fluxes of CO_2 in three Arctic seas: A sensitivity study using Earth observation. *Biogeosciences*, *10*, 8109–8128. https://doi.org/10.5194/bg-10-8109-2013

Lauvset, S. K., Chierici, M., Counillon, F., Omar, A., Nondal, G., Johannessen, T., & Olsen, A. (2013). Annual and seasonal fCO_2 and air-sea CO_2 fluxes in the Barents Sea. *Journal of Marine Systems*, *113-114*, 62–74. https://doi.org/10.1016/j.jmarsys.2012.12.011

Lewis, E., & Wallace, D. W. R. (1998). *Program developed for CO_2 system calculations, ORNL/CDIAC-105*, CDIAC. Oak Ridge, Tennessee: Oak Ridge Natl. La.b.

Lueker, T. J., Dickson, A. G., & Keeling, C. D. (2000). Ocean pCO_2 calculated from dissolved inorganic carbon, alkalinity, and equations for K_1 and K_2: Validation based on laboratory measurements of CO_2 in gas and seawater at equilibrium. *Marine Chemistry*, *70*(1–3), 105–119. https://doi.org/10.1016/S0304-4203(00)00022-0

Lüger, H., Wallace, D. W. R., Körtzinger, A., & Nojiri, Y. (2004). The pCO_2 variability in the midlatitude North Atlantic Ocean during a full annual cycle. *Global Biogeochemical Cycles*, *18*, GB3023. https://doi.org/10.1029/2003GB002200

Mehrbach, C., Culberson, C. H., Hawley, J. E., & Pytkowicz, R. M. (1973). Measurement of the apparent dissociation constants of carbonic acid in seawater at atmospheric pressure. *Limnology and Oceanography*, *18*, 897–907. https://doi.org/10.4319/lo.1973.18.6.0897

Meire, L., Søgaard, D. H., Mortensen, J., Meysman, F. J. R., Soetaert, K., Arendt, K. E., et al. (2015). Glacial meltwater and primary production are drivers of strong CO_2 uptake in fjord and coastal waters adjacent to the Greenland Ice Sheet. *Biogeosciences*, *12*(8), 2347–2363. https://doi.org/10.5194/bg-12-2347-2015

Millero, F. J. (1979). The thermodynamics of the carbonate system in seawater. *Geochimica et Cosmochimica Acta*, *43*(10), 1651–1661. https://doi.org/10.1016/0016-7037(79)90184-4

Muckenhuber, S., Nilsen, F., Korosov, A., & Sandven, S. (2016). Sea ice cover in Isfjorden and Hornsund, Svalbard (2000-2014) from remote sensing data. *The Cryosphere*, *10*(1), 149–158. https://doi.org/10.5194/tc-10-149-2016

Nakaoka, S.-I., Aoki, S., Nakazawa, T., Hashida, G., Morimoto, S., Yamanouchi, T., & Yoshikawa-Inoue, H. (2006). Temporal and spatial variations of oceanic pCO_2 and air-sea CO_2 flux in the Greenland Sea and the Barents Sea. *Tellus Series B: Chemical and Physical Meteorology*, *58*(2), 148–161. https://doi.org/10.1111/j.1600-0889.2006.00178.x

Nightingale, P. D., Malin, G., Law, C. S., Watson, A. J., Liss, P. S., Liddicoat, M. I., et al. (2000). In situ evaluation of the air–sea gas exchange parameterizations using novel conservative and volatile tracers. *Global Biogeochemical Cycles*, *14*(1), 373–387. https://doi.org/10.1029/1999GB900091

Nilsen, F., Cottier, F., Skogseth, R., & Mattsson, S. (2008). Fjord-shelf exchanges controlled by ice and brine production: The interannual variation of Atlantic Water in Isfjorden, Svalbard. *Continental Shelf Research*, *28*(14), 1838–1853. https://doi.org/10.1016/j.csr.2008.04.015

Nilsen, F., Skogseth, R., Vaardal-Lunde, J., & Inall, M. (2016). A simple shelf circulation model: Intrusion of Atlantic Water on the West Spitsbergen Shelf. *Journal of Physical Oceanography*, *46*(4), 1209–1230. https://doi.org/10.1175/JPO-D-15-0058.1

Omar, A. M., Johannessen, T., Olsen, A., Kaltin, S., & Rey, F. (2007). Seasonal and interannual variability of the air-sea CO_2 flux in the Atlantic sector of the Barents Sea. *Marine Chemistry*, *104*(3-4), 203–213. https://doi.org/10.1016/j.marchem.2006.11.002

Onarheim, I. H., Smedsrud, L. H., Ingvaldsen, R. B., & Nilsen, F. (2014). Loss of sea ice during winter north of Svalbard. *Tellus Series A*, *66*(1), 23933. https://doi.org/10.3402/tellusa.v66.23933

Pavlov, A. K., Tverberg, V., Ivanov, B. V., Nilsen, F., Falk-Petersen, S., & Granskog, M. A. (2013). Warming of Atlantic water in two West Spitsbergen fjords over the last century (1912-2009). *Polar Research*, *32*, 11206. https://doi.org/10.3402/polar.v32i0.1

Pipko, I. I., Semiletov, I. P., Pugach, S. P., Wåhlström, I., & Anderson, L. G. (2011). Interannual variability of air-sea CO_2 fluxes and carbon system in the East Siberian Sea. *Biogeosciences*, *8*(7), 1987–2007. https://doi.org/10.5194/bg-8-1987-2011

Randelhoff, A., Fer, I., & Sundfjord, A. (2017). Turbulent upper-ocean mixing affected by meltwater layers during Arctic summer. *Journal of Physical Oceanography*, *47*(4), 835–853. https://doi.org/10.1175/JPO-D-16-0200.1

Redfield, A. C., Ketchum, B. H., & Richards, F. A. (1963). The influence of organisms on the composition of sea-water. In M. N. Hill (Ed.), *The sea: Ideas and observations on the progress in the study of the seas* (Vol. 2, pp. 26–77). New York: Interscience.

Rysgaard, S., Mortensen, J., Juul-Pedersen, T., Sørensen, L. L., Lennert, K., Søgaard, D. H., et al. (2012). High air–sea CO_2 uptake rates in nearshore and shelf areas of Southern Greenland: Temporal and spatial variability. *Marine Chemistry*, *128-129*, 26–33. https://doi.org/10.1016/j.marchem.2011.11.002

Sarmiento, J. L., & Gruber, N. (2006). *Ocean biogeochemical dynamics*. Princeton, NJ, USA: Princeton University Press.

Sejr, M. K., Krause-Jensen, D., Rysgaard, S., Sørensen, L. L., Christensen, P. B., & Glud, R. N. (2011). Air-sea flux of CO_2 in arctic coastal waters influenced by glacial melt water and sea ice. *Tellus Series B*, *63*(5), 815–822. https://doi.org/10.1111/j.1600-0889.2011.00540.x

Semiletov, I. P., Pipko, I. I., Repina, I., & Shakhova, N. E. (2007). Carbonate chemistry dynamics and carbon dioxide fluxes across the atmosphere-ice-water interfaces in the Arctic Ocean: Pacific sector of the Arctic. *Journal of Marine Systems*, *66*(1–4), 204–226. https://doi.org/10.1016/j.jmarsys.2006.05.012

Svendsen, H., Beszczynska-Møller, A., Hagen, J. O., Lefauconnier, B., Tverberg, V., Gerland, S., et al. (2002). The physical environment of Kongsfjorden-Krossfjorden, an Arctic fjord system in Svalbard. *Polar Research*, *21*(1), 133–166.

Sweeney, C., Gloor, E., Jacobson, A. R., Key, R. M., McKinley, G., Sarmiento, J. L., & Wanninkhof, R. (2007). Constraining global air-sea gas exchange for CO_2 with recent bomb ^{14}C measurements. *Global Biogeochemical Cycles*, *21*, GB2015. https://doi.org/10.1029/2006GB002784

Takahashi, T., Olafsson, J., Goddard, J. G., Chipman, D. W., & Sutherland, S. C. (1993). Seasonal variation of CO_2 and nutrients in the high latitude surface oceans: A comparative study. *Global Biogeochemical Cycles*, *7*(4), 843–878. https://doi.org/10.1029/93GB02263

Takahashi, T., Sutherland, S. C., Wanninkhof, R., Sweeney, C., Feely, R. A., Chipman, D. W., et al. (2009). Climatological mean and decadal change in surface ocean pCO_2, and net sea–air CO_2 flux over the global oceans. *Deep Sea Research Part II*, *56*(8–10), 554–577. https://doi.org/10.1016/j.dsr2.2008.12.009

Uppström, L. R. (1974). The boron/chlorinity ratio of deep-sea water from the Pacific Ocean. *Deep Sea Research and Oceanographic Abstracts*, *21*(2), 161–162. https://doi.org/10.1016/0011-7471(74)90074-6

van Heuven, S., Pierrot, D., Rae, J. W. B., Lewis, E., & Wallace, D. W. R. (2011). MATLAB program developed for CO_2 system calculations, rep. ORNL/CDIAC-105b, carbon dioxide Inf. Anal. Cent., Oak Ridge, Tenn. https://doi.org/10.3334/CDIAC/otg.CO2SYS_MATLAB_v1.1

Wanninkhof, R. (2014). Relationship between wind speed and gas exchange over the ocean revisited. *Limnology and Oceanography: Methods*, *12*(6), 351–362. https://doi.org/10.4319/lom.2014.12.351

Wanninkhof, R. H. (1992). Relationship between wind speed and gas exchange over the ocean. *Journal of Geophysical Research*, *97*(C5), 7373–7382. https://doi.org/10.1029/92JC00188

Wanninkhof, R. H., Asher, W. E., Ho, D. T., Sweeney, C., & McGillis, W. R. (2009). Advances in quantifying air-sea gas exchange and environmental forcing. *Annual Review of Marine Science*, *1*(1), 213–244. https://doi.org/10.1146/annurev.marine.010908.163742

Weiss, R. F. (1974). Carbon dioxide in water and seawater: The solubility of a non-ideal gas. *Marine Chemistry*, *2*(3), 203–215. https://doi.org/10.1016/0304-4203(74)90015-2

Woosley, R. J., Millero, F. J., & Takahashi, T. (2017). Internal consistency of the inorganic carbon system in the Arctic Ocean. *Limnology and Oceanography: Methods*, *15*(10), 887–896. https://doi.org/10.1002/lom3.10208

World Meteorological Organization (2014). *Guide to Meteorological Instruments and Methods of Observation (WMO-No 8)*. Geneva, Switzerland: World Meteorological Organization.

Wynn, P. M., Hodson, A. J., Heaton, T. H. E., & Chenery, S. R. (2007). Nitrate production beneath High Arctic glacier, Svalbard. *Chemical Geology*, *244*(1–2), 88–102. https://doi.org/10.1016/j.chemgeo.2007.06.008

Yasunaka, S., Murata, A., Watanabe, E., Chierici, M., Fransson, A., van Heuven, S., et al. (2016). Mapping of the air-sea CO_2 flux in the Arctic Ocean and its adjacent seas: Basin-wide distribution and seasonal to interannual variability. *Polar Science*, *10*(3), 323–334. https://doi.org/10.1016/j.polar.2016.03.006